Crystallographic Investigation of the Inhibition Mode of a VIM-2 Metallo-β-lactamase from *Pseudomonas aeruginosa* by a Mercaptocarboxylate Inhibitor

Yoshihiro Yamaguchi,*[,§,⊥] Wanchun Jin,[‡] Kazuyo Matsunaga,[‡] Shinnji Ikemizu,[¶] Yuriko Yamagata,[¶] Jun-ichi Wachino,[†] Naohiro Shibata,[†] Yoshichika Arakawa,[†] and Hiromasa Kurosaki*[,‡,⊥]

Environmental Safety Center, Kumamoto University, 39-1 Kurokami 2-Chome, Kumamoto 860-8555, Japan, Departments of Structure-Function Physical Chemistry and Structural Biology, Graduate School of Pharmaceutical Sciences, Kumamoto University, Oe-honmachi 5-1, Kumamoto 862-0973, Japan, and Department of Bacterial Pathogenesis and Infection Control, National Institute of Infectious Diseases, 4-7-1 Gakuen, Musashi-Murayama, Tokyo 208-0011, Japan

Received August 19, 2007

The VIM-2 metallo-β-lactamase enzyme from *Pseudomonas aeruginosa* catalyzes the hydrolysis of most β-lactam antibiotics including carbapenems, and there are currently no potent inhibitors of such enzymes. We found *rac*-2-ω-phenylpropyl-3-mercaptopropionic acid, phenylC3SH, to be a potent inhibitor of VIM-2. The structure of the VIM-2−phenylC3SH complex was determined by X-ray crystallography to 2.3 Å. The structure revealed that the thiol group of phenylC3SH bridged to the two zinc(II) ions and the phenyl group interacted with Tyr67(47) on loop1 near the active site, by $\pi-\pi$ stacking interactions. The methylene group interacted with Phe61(42) located at the bottom of loop1 through CH$-\pi$ interactions. Dynamic movements were observed in Arg228(185) and Asn233(190) on loop2, compared with the native structure (PDB code: 1KO3). These results suggest that the above-mentioned four residues play important roles in the binding and recognition of inhibitors or substrates and in stabilizing a loop in the VIM-2 enzyme.

Introduction

β-Lactamases catalyze the hydrolysis of the C−N bond of the β-lactam ring in β-lactam antibiotics, rendering them inactive.[1,2] In the family of β-lactamases, four molecular classes, A−D, were defined on the basis of their amino acid sequence homologies.[3–5] Classes A, C, and D are serine β-lactamases containing a serine residue at the active site, whereas class B metallo-β-lactamases (MBLs[a]) contain one or two zinc(II) ions at the active site. Moreover, MBLs are classified into three subclasses:[6,7] subclass B1 including BcII,[8] an IMP family (IMP-1 to IMP-18),[9] CcrA,[10] and a VIM family (VIM-1 to VIM-11a and -11b);[9] subclass B2 including CphA[11] and ImiS;[12] and subclass B3 including L1[13] and THIN-B.[14] Of all the MBLs, the VIM family and the IMP family are emerging as a worldwide source of acquired carbapenem resistance among Gram-negative bacteria. In variants of VIMs, VIM-2 was first detected from *Pseudomonas aeruginosa* in France in 1996[15] and is now one of the most widespread enzymes in well-known MBLs. The VIM-2 enzyme shows a 24–31% identity with other subclass B1 MBLs such as BlaB, CcrA, and IMP-1.[15]

The $bla_{\text{VIM-2}}$ gene is located in a mobile plasmid-encoded gene cassette inserted into the variable region of an integron structure so that horizontal spread of resistance is possible. In fact, $bla_{\text{VIM-2}}$ genes have been detected mostly in the Mediterranean countries of Europe, in the Far East regions, including Japan, and at present, in American regions, including the U.S., whereas $bla_{\text{IMP-1}}$ genes were first detected mainly in Japan and subsequently isolated in Asia, Europe, and South America.[9] Moreover, in addition to the high resistance against β-lactam antibiotics, there are no clinically available inhibitors for the VIM-2 enzyme including other MBLs at present. Thus, the development of inhibitors is an important subject. The active site in an MBL is made up of the zinc(II) ion(s), the zinc(II) ion binding residues, and two loops. In the two loops, the first loop (loop1) is composed of two β-sheets and a turn constitutes a β-sheet flap, whereas the second loop (loop2) is approximately positioned in the opposite site of loop1 centered about the zinc(II) ion binding site. It is thought that these loops are responsible for substrate recognition, binding, and catalysis in MBLs.[16–22]

To develop potent and common inhibitors, it is necessary to focus on the structure and dynamics of both the zinc(II) ion binding site and loops 1 and 2 in each MBL and its complex with a lead compound.

So far, X-ray crystal structures of MBLs complexed with various inhibitors have been reported with the exception of the VIM-2 enzyme: CcrA−4-morpholineethanesulfonic acid,[23] CcrA−biphenyltetrazoles,[24] IMP-1−mercaptocarboxylate derivative,[22] IMP-1–2,3-disubstituted succinic acid derivatives,[25] IMP-1−irreversible thiol compound with a good leaving group,[26] IMP-1−dansylC4SH,[27] BlaB−D-captopril,[28] and FEZ−D-captopril.[29]

In VIM-2, in 2001, García-Sáez et al. deposited two X-ray crystal structures of VIM-2 in the reduced (denoted as the native VIM-2 enzyme) and oxidized forms of Cys221(178) from *P. aerginosa* into the Protein Data Bank (PDB codes 1KO2 and 1KO3). As far as we know, however, detailed information on the structure of the VIM-2 enzyme complexed with an inhibitor is not available.

* To whom correspondence should be addressed. For Y.Y.: phone, +81-96-342-3238; fax, +81-96-342-3237; e-mail, yyamagu@gpo.kumamoto-u.ac.jp. For H.K.: phone and fax, +81-96-371-4314; e-mail, ayasaya@gpo.kumamoto-u.ac.jp.

§ Environmental Safety Center, Kumamoto University.

⊥ These authors contributed equally to work.

‡ Department of Structure-Function Physical Chemistry, Kumamoto University.

¶ Department of Structural Biology, Kumamoto University.

† National Institute of Infectious Diseases.

[a] Abbreviations: BBL, class B β-lactamase; MAD, multiwavelength anomalous dispersion; MBLs, metallo-β-lactamases; PEG MME5000, polyethylene glycol monomethyl ether 5000; phenylC3SH, 2-ω-phenylpropyl-3-mercaptopropionic acid. In this paper, the amino acid residues of metallo-β-lactamase are designated with the BBL number and the amino acid sequence number by putting the latter in parentheses.

10.1021/jm701031n CCC: $37.00
Published on Web 12/06/2007

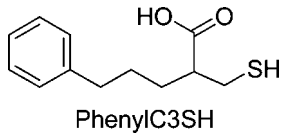

PhenylC3SH

Figure 1. Structure of *rac*-2-ω-phenylpropyl-3-mercaptopropionic acid, phenylC3SH.

We are currently in the process of synthesizing several inhibitors and screening them for inhibitory activity against the VIM-2 and IMP-1 enzymes for the purpose of developing inhibitors for MBLs. In this process, the mercaptocarboxylate inhibitor, PhenylC3SH (Figure 1), was found to be a potent inhibitor of the VIM-2 enzyme with a K_i value of 220 nM, whereas it is less active for the IMP-1 enzyme (K_i = 1660 nM).[30]

For the purpose of understanding structure–activity relationships of the VIM-2 enzyme with respect to phenylC3SH, we carried out X-ray crystallography of the VIM-2 enzyme complexed with phenylC3SH.

Here, we report on the X-ray crystal structure of the VIM-2 enzyme from *P. aeruginosa* complexed with phenylC3SH determined at a resolution of 2.3 Å.

Results and Discussion

In this study, we determined the crystal structure of the VIM-2 enzyme complexed with phenylC3SH in order to elucidate the detailed binding mode of the inhibitor with the enzyme, in particular, focusing on the role of the mobile loop, along with a comparison of the native VIM-2 structure (PDB code 1KO3).

Overall Structure of the VIM-2 Enzyme Complexed with PhenylC3SH. The final refined structural model contained two VIM-2−phenylC3SH molecules in an asymmetric unit, consisting of Glu30(12)−Val290(236) residue each for molecules A and B. The root-mean-squared deviation (rmsd) value between the α-carbon atoms of the two monomers was about 0.28 Å. In molecules A and B, two zinc(II) ions and one phenylC3SH molecule are located at the active sites. The final $R_{working}$ and R_{free} values were 0.212 and 0.247, respectively, and the rmsd values from ideal bond distances and angles were 0.007 Å and 2.0°, respectively (Table 1). The overall structure of the inhibitor complex adopts an $\alpha\beta/\beta\alpha$ sandwich structure, where the active site containing the two zinc(II) ions is located at the bottom at the interface of the two β-sheets surrounded by two α-helices, which resemble those of other subclass B1 MBLs.[22,28,31]

In addition, a clear electron density corresponding to a phenylC3SH molecule was found in the active center (Figures 2 and 3). Although the crystals were grown in the presence of a racemic mixture of phenylC3SH, only the *S*-isomer of the inhibitor was observed in the complex.

All main chain dihedral angles were within the allowed regions of a Ramachandran plot except Asp84(64) and Ala195(158) which adopted φ, ψ angles of 73/74° (molecules A/B), 151/149°, and −151/−157°, −106/−106°, respectively. Asp84(64) is buried in the protein, whereas Ala195(158) is positioned on top of a hairpin loop formed from Tyr191(154)−Val202(165). Asp84(64) and Ala195(158) have strained main chain conformations in both the native VIM-2 enzyme and the phenylC3SH complex. In the crystal structures of BcII, CcrA, and IMP-1 metallo-β-lactamases,[22,31,32] Asp84s were found to have a common strained conformation. Therefore, the conservation of the conformation of Asp84 suggests that it is important for the folding of metallo-β-lactamases. In additional supporting evidence, tRNA maturase RNase Z (PDB code 1Y44)[33] and pre-mRNA 3′-end-processing endonuclease CPSF-73 (PDB code 2I7T)[34] in the metallo-β-lactamase family also have strained main chain conformations of the Asp residues, as has been found for Asp84 of MBLs.

The structures of molecule A in an asymmetric unit of the phenylC3SH complex and that of the native VIM-2 enzyme (PDB code 1KO3) are superimposable except for residues Lys291(237)−Asn295(241), and the rmsd for the α-carbon atoms between them was 0.56 Å. In a comparison of the deviations of the α-carbon atoms between each of the amino acid residues of the native VIM-2 enzyme and the inhibitor complex, residues that moved more than 1 Å were Val34(16) (1.4 Å), Ser35(17) (2.7 Å), Glu36(18) (2.3 Å), Ile37(19) (1.0 Å), Pro38(20) (1.2 Å), Val39(21) (1.1 Å), Ser60(41) (1.5 Å), Phe61(42) (1.8 Å), Asp62(43) (1.9 Å), Gly63(44) (2.0 Å), Ala64(45) (1.4 Å), Val66(46) (1.2 Å), and Gly232(189) (1.8 Å), respectively.

Of these residues, Val34(16), Ser35(17), Glu36(18), Ile37(19), Pro38(20), and Val39(21) were located at the N terminus and Ser60(41), Phe61(42), Asp62(43), Gly63(44) (2.3 Å), Ala64(45), and Val66(46) were located on loop1, whereas Gly232(189) was located on loop2.

Active Site of the VIM-2 Enzyme Complexed with PhenylC3SH. In the phenylC3SH complex, one of two zinc(II) ions (Zn1) was coordinated to His116(94), His118(96), and His196(159) residues with distances of 2.2/2.1 Å (in molecules A/B), 2.0/2.2 Å, and 2.2/2.2 Å, respectively.

The thiol group of the inhibitor is bridged to the two zinc(II) ions (the distances of Zn1−S and Zn2−S were 2.5/2.2 Å and 2.1/2.2 Å), respectively, forming a tetrahedral coordination around the Zn1 atom (the average angle of ligand−Zn1−ligand is 109° for molecule A and 110° for molecule B; Figure 3, Table 2). The coordination of the thiol group of an inhibitor to two zinc(II) ions is similar to those found in IMP-1 complexed with 2-[5-(1-tetrazoylmethyl)thien-3-yl]-*N*-[2-(mercaptomethyl)-4-(phenylbutyrylglycine)][22] or with dansylC4SH[27] and in BlaB complexed with D-captopril.[28]

The second zinc(II) ion (Zn2) is also tetrahedrally coordinated by Asp120(98), Cys221(178), and His263(220) residues, and the thiol group of the inhibitor with distances of 1.9/2.0, 2.2/2.2, 2.1/2.1, and 2.1/2.2 Å, respectively (the average angles of ligand−Zn2−ligand is 109° for molecules A and B, respectively; Figure 3, Table 2). The Zn1−Zn2 distance is 3.8 Å for molecule A and 3.7 Å for molecule B, and this distance is close to those found in the IMP-1 and BlaB enzymes in complex with an inhibitor containing a thiol group (the average distance of 3.6–3.7 Å).[22,27,28]

In the native VIM-2 structure, the geometry around the Zn1 atom is a distorted tetrahedral with three His residues (His116(94), His118(96), and His196(159)) and H_2O/or OH^- (this H_2O/or OH^- is thought to act as the attacking nucleophile on the carbonyl carbon atom of the β-lactam ring),[31,35,36] bridging to the Zn1 and Zn2 atoms, whereas that around the Zn2 atom is a distorted square-pyramid with the basal plane defined by a H_2O/or OH^-, Asp120(98), Cys221(178), His263(220), and Cl atom, where the Cl atom interacts weakly with the Zn2 atom with a distance of 2.9 Å. The apical position is occupied by Asp120(98). In the crystal structures of other subclass B1 MBLs (CcrA and IMP-1),[22,31] the Cl atom in the Zn2 site of the native VIM-2 enzyme is replaced by H_2O, which is thought to contribute to the catalysis of the hydrolysis of β-lactam antibiotics.[31,37] Unlike the native VIM-2 enzyme, the coordination geometry around the Zn2 atom in CcrA and IMP-1 is a distorted trigonal bipyramid.

Table 1. Crystallographic Data Collection and Refinement Statistics for the VIM-2 Enzyme Complexed with PhenylC3SH

data collection				
data set wavelength (Å)	1.0000 (final)	1.2826 (edge)	1.2817 (peak)	1.2906 (remote)
resolution (outer shell) (Å)	50.0–2.30 (2.38–2.30)	99.0–2.53 (2.63–2.53)	99.0–2.54 (2.63–2.54)	99.0–2.55 (2.65–2.55)
cell dimensions				
a, *b*, and *c* (Å)	45.2, 90.75, 129.0			
space group	$P2_12_12_1$			
molecules/asymmetric unit	2			
completeness (outer shell) (%)	99.6 (98.4)	99.2 (96.3)	99.1 (96.7)	99.0 (94.8)
R_{merge}[a] (outer shell)	0.062 (0.267)	0.047 (0.106)	0.050 (0.097)	0.046 (0.121)
no. of observed reflns	163206	123781	122809	121255
no. of unique reflns	24156	18155	18121	17742
$\langle I/(\sigma)\rangle$ (outer shell)	34.9 (4.45)	54.2 (25.5)	55.5 (30.1)	53.4 (23.3)
refinement statistics				
resolution (Å)	42.8–2.30			
no. of non-H atoms[b]				
protein	3392			
ligand	50			
water	212			
rmsd from ideal[c]				
bond length (Å)	0.007			
angles (deg)	2.0			
$R_{working}$[d]	0.212			
R_{free}[e]	0.247			

[a] $R_{merge} = \sum|I_j - \langle I_j\rangle|/\sum I_j$, where I_j is the observed intensity for reflection j and $\langle I_j\rangle$ is the average intensity calculated for reflection j from replicate data. [b] Per asymmetric unit. [c] rmsd: root-mean-square-deviation. [d] $R_{working} = \sum||F_o| - |F_c||/\sum|F_o|$, where F_o and F_c are the observed and calculated structure factors, respectively. [e] $R_{free} = \sum||F_o| - |F_c||/\sum|F_o|$ for 5% of the data not used at any stage of structural refinement.

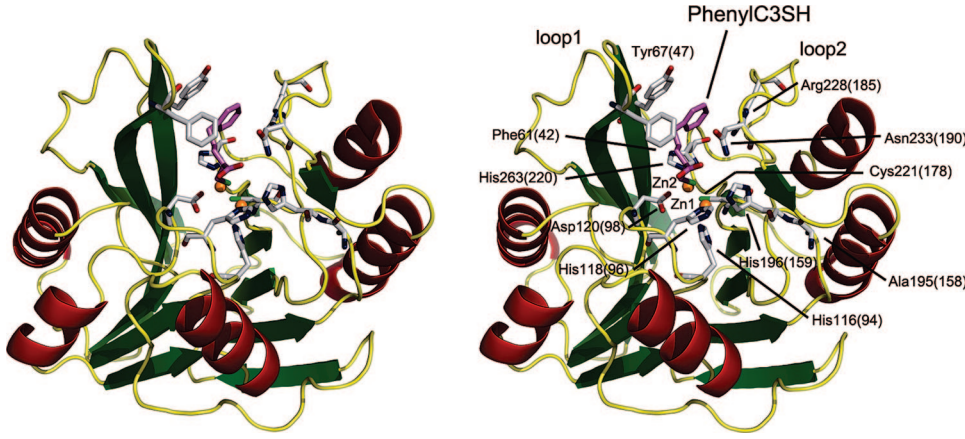

Figure 2. Overall structure of the VIM-2 enzyme from *P. aerginosa* is complexed with phenylC3SH. Molecule A of the phenylC3SH complex is depicted, and the amino acid residues of VIM-2 are designated by a BBL number and an amino acid sequence number; the latter is in parentheses. α-Helices, β-strands, and loops are shown in red, green, and yellow, respectively. Zn(II) atoms are shown as orange spheres. Carbon, oxygen, and sulfur atoms in phenylC3SH are shown as magenta, red, and light-green sticks, respectively. The figure was prepared with PyMol software (http://pymol.sourceforgen.net/).

Comparison of Loop between the Native VIM-2 Enzyme and the PhenylC3SH Complex. The VIM-2 enzyme contains loop1 (Phe61(42)−Ala64(45)) and loop2 (Ile223(180)−Trp242(199)).

Upon inhibitor binding, significant structural changes were found in both loops. The amino acid residues on loop1 are thought to be the most important for substrate recognition and binding, catalysis, and inhibition.[16–19,22] In the phenylC3SH complex, Tyr67(47) and Phe61(42), located on loop1, moved toward the active site to facilitate the interaction with the inhibitor (Figure 4). Compared to the native VIM-2 structure, Tyr67(47) rotates by ∼27° about the Cβ−Cγ bond of Tyr67(47) to provide face-to-face π−π stacking interactions between the phenyl rings of the inhibitor and Tyr67(47) with spacing planes of ∼3.6 Å (Figures 3 and 4). At the same time, the phenyl ring of Phe61(42) lie ∼1.3 Å closer to Zn2 (Figure 4), forming CH−π interactions with the methylene chain of the inhibitor, and these interactions may contribute to the stabilization of loop1. In addition, the active site of the phenylC3SH complex is transformed from an opened cavity into a tunnel-shaped cavity upon binding of an inhibitor (Figure 5).

In loop2 of the phenylC3SH complex, the carboxyl group (O2) of the inhibitor interacts through a hydrogen bond with the side chain ND2 of Asn233(190) (2.9/2.6 Å in molecules A/B), which is conserved in most MBLs.[36] A comparison of the structures between the native VIM-2 and the inhibitor complex showed that conformational change in Asn233(190) is accomplished by the rotation of the neighboring amino acid Gly232(189) (φ and ψ angles are −85° and −119°, respectively, for the native VIM-2 enzyme, whereas those of the phenylC3SH complex are 73° and −143° for molecule A and 63° and −143° for molecule B, respectively; Figure 4). In addition, the binding of the inhibitor to the active site triggers a conformational change in the side chain Arg228(185) (Figure 4): the torsion angle of CB−CG−CD−NE of Arg228(185) is changed from −48° in the native VIM-2 enzyme to 172° for molecule A and −175° for molecule B, respectively, in the phenylC3SH complex. These results suggest that Phe61(42), Tyr67(47), Arg228(185), and Asn233(190) are functionally important residues that play roles in the binding and recognition of the inhibitor or substrate and in stabilizing loops 1 and 2.

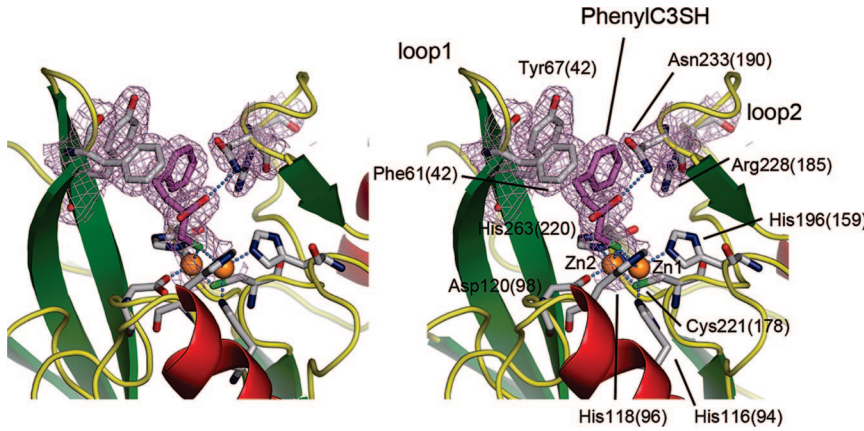

Figure 3. Stereoview of the active site of the VIM-2 enzyme complexed with phenylC3SH. Molecule A of the phenylC3SH complex is depicted, and the amino acid residues of VIM-2 are labeled with a BBL number and an amino acid sequence number; the latter is in parentheses. The electron density map (pink mesh) of phenylC3SH is shown contoured at the 1.0σ level in the $2|F_o| - |F_c|$ map. Zn(II) atoms are shown as orange spheres. Phe61(42), Tyr67(47), His116(94), His118(96), His196(159), His263(220), Asp120(98), Cys221(178), Arg228(185), and Asn233(190) residues and phenylC3SH are represented as sticks. Carbon atoms in amino acid residues are shown in gray (nitrogen, blue; oxygen, red; and sulfur, light-green), and carbon atoms in phenylC3SH are shown in magenta (oxygen, red; sulfur, light-green). The figure was prepared with PyMol software (http://pymol.sourceforgen.net/).

Table 2. Zinc(II)−Ligand Distances (Å) and Angles (deg) for the Native VIM-2 Enzyme and the PhenylC3SH Complex

		distance	
Zn(II)−ligand		native VIM-2	VIM-2−phenylC3SH complex[a]
Zn1	His116(94)NE2	2.2	2.0/2.1
	His118(96)ND1	2.1	2.0/2.2
	His196(159)NE2	2.2	2.2/2.2
	O(w)	2.1	
	S(phenylC3SH)		2.5/2.2
Zn2	Asp120(98)OD2	2.3	1.9/2.0
	Cys221(178)SG	2.3	2.2/2.2
	His263(220)NE2	2.3	2.1/2.1
	O(w)	2.5	
	S(phenylC3SH)		2.1/2.2
	Cl	2.9	
Zn1	Zn2	4.2	3.8/3.7

			angle	
ligand−Zn(II)−ligand			native VIM-2	VIM-2−phenylC3SH complex[a]
His116(94)NE2	Zn1	His118(96)ND1	103	105/105
	Zn1	His196(96)NE2	103	120/110
	Zn1	O(w)	103	
	Zn1	S(inhibitor)		116/126
His118(96)ND1	Zn1	His196(159)NE2	116	101/107
	Zn1	O(w)	119	
	Zn1	S(inhibitor)		113/112
His196(159)NE2	Zn1	O(w)	111	
	Zn1	S(inhibitor)		101/97
Asp120(98)OD2	Zn2	Cys221(178)SG	103	114/117
	Zn2	His263(220)NE2	94	96/99
	Zn2	O(w)	74	
	Zn2	S(inhibitor)		100/100
	Zn	Cl	101	
Cys221(178)SG	Zn2	His263(220)NE2	103	104/105
	Zn2	O(w)	98	
	Zn2	S(inhibitor)		124/116
	Zn2	Cl	152	
His263(220)NE2	Zn2	O(w)	157	
	Zn2	S(inhibitor)		116/119
	Zn2	Cl	103	

[a] The distances and angles for the phenylC3SH complex are quoted for molecules A and B in the asymmetric unit.

Comparison of Loops 1 and 2 between the IMP-1 and VIM-2 Enzymes. We compared the amino acid residues on loops 1 and 2 between the VIM-2 and IMP-1 enzymes (Figure 6). In the case of the IMP-1 enzyme,[22] Trp64(28) is located on the top of loop1, and this residue is thought to be important for the binding of both inhibitors and substrates. Indeed, the role of Trp64(28) in the binding of inhibitors has been demonstrated in X-ray crystal structures of the IMP-1−mercaptocarboxylate inhibitor and −dansylC4SH complexes; the indole ring of Tyr64(28) interacts with the aromatic ring of the inhibitor, and this interaction causes a dynamic movement of loop1 to cover an inhibitor into the active site.[22,27] On the other hand, Trp64(28) in the IMP-1 enzyme is replaced with Ala64(45) in the VIM-2 enzyme. Therefore, in the VIM-2 enzyme, Trp64(28) in IMP-1 is covered with the hydrophobic residues Phe61(42) and Tyr67(47) located in the root of the loop1. Phe61(42) and Tyr67(47) in the VIM-2 enzyme are replaced by Val61(25) and Val67(31), respectively, in the IMP-1 enzyme. It is thought that these residues could not participate in hydrophobic contacts with the inhibitor seen in the crystal structure of the phenylC3SH complex, reflecting the difference

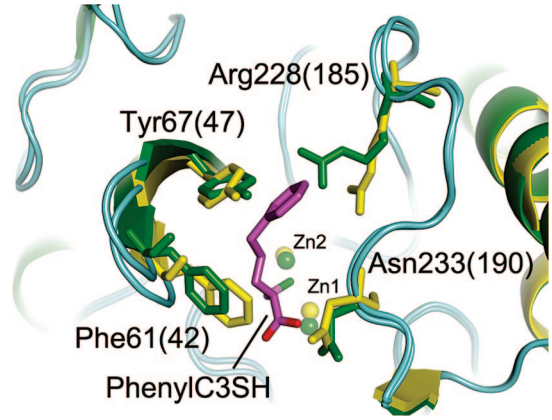

Figure 4. Conformational changes in loops 1 and 2 upon phenylC3SH binding to the VIM-2 enzyme. Superposition of native VIM-2 (green) (PDB code 1KO3) and the phenylC3SH complex (yellow). Molecule A of the phenylC3SH complex is depicted and the amino acid residues of VIM-2 are designated with a BBL number and an amino acid sequence number; the latter is in parentheses. Phe61(42), Tyr67(47), Arg228(185), and Asn233(190) residues are presented as balls and sticks. Zn(II) ions are shown as orange spheres. PhenylC3SH is presented as a stick (carbon, oxygen, and sulfur atoms are shown in magenta, red, and light-green, respectively). The figure was prepared with PyMol software (http://pymol.sourceforgen.net/).

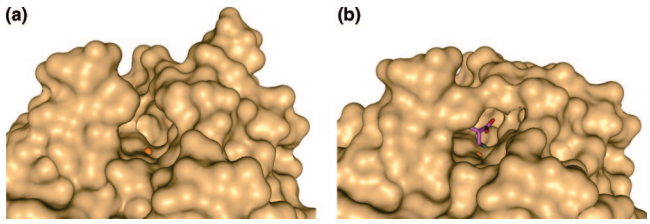

Figure 5. Molecular surface representations of native VIM-2 (a) and the phenylC3SH complex (b). In the phenylC3SH complex, molecule A is depicted as a molecular surface. The amino acid residues of VIM-2 are designated with a BBL number and an amino acid sequence number; the latter is in parentheses. Zn(II) ion (Zn2) is shown as an orange sphere. PhenylC3SH is presented as a stick (carbon, oxygen, and sulfur atoms are shown in magenta, red, and light-green, respectively). The figure was prepared with PyMol software (http://pymol.sourceforgen.net/).

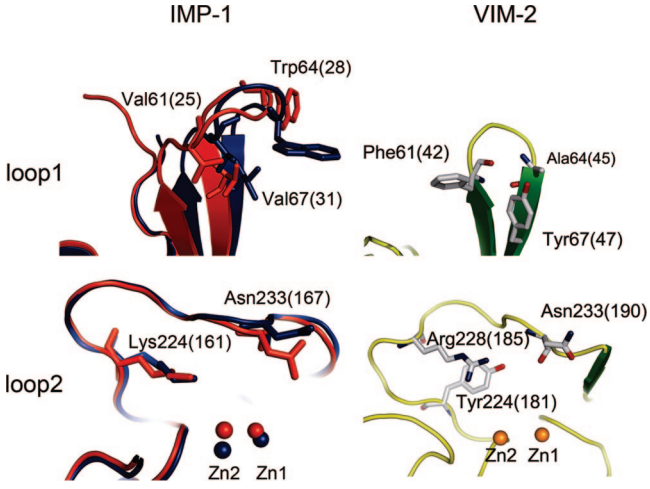

Figure 6. Comparison of loops 1 and 2 between IMP-1 and VIM-2 enzymes. The amino acid residues of the IMP-1 and VIM-2 enzymes are designated with a BBL number and an amino acid sequence number; the latter is in parentheses. In the IMP-1 enzyme (left), the structures of IMP-1 metallo-β-lactamase from *P. aeruginosa* (PDB code 1DDK) (red) and its complex with a mercaptocarboxylate inhibitor (PDB code 1DD6, molecule A is depicted) (blue) were used for comparison,[22] but the inhibitor 2-[5-(1-tetrazoylmethyl)thien-3-yl]-*N*-[2-(mercaptomethyl)-4-(phenylbutyrylglycine)] was omitted for clarity. Val61(25), Trp64(28), and Val67(31) residues on loop1 and Lys224(161) and Asn233(167) residues on loop2 are presented as sticks (carbon, gray; nitrogen, blue; oxygen, red). Zn(II) ions are shown as orange spheres. In the VIM-2−phenylC3SH complex (right), molecule A is depicted and phenylC3SH was omitted for clarity. Phe61(42), Ala64(45), and Tyr67(47) residues on loop1 and Tyr224(181), Arg228(185), and Asn233(190) residues of the VIM-2 enzyme are presented as sticks (carbon, gray; nitrogen, blue; oxygen, red). Zn(II) ions are shown as orange spheres. The figure was prepared with the PyMol software program (http://pymol.sourceforgen.net/).

in inhibitory activity of phenylC3SH between the VIM-2 and IMP-1 enzymes.

Lys224(161) in the IMP-1 enzyme is located on loop2, which is ~5 Å away from the Zn(II) center. In the mercaptocarboxylate inhibitor complex, the carboxyl group of inhibitor interacts with the side chain NZ of Lys224(161) with a distance of 2.8 Å, and this result shows the importance of Lys224(161) in inhibitor binding. Moreover, Lys224(161) is assumed to interact with the carboxylate of the β-lactam antibiotics.[22,31] However, in the case of the VIM-2 enzyme, Lys224(161) is replaced with Tyr224(181). On the basis of the crystal structure of the phenylC3SH complex, Arg228(185) near Tyr224(181) on loop2 might aid in carrying out the role of Lys224(161) in IMP-1.

It is noteworthy that the movement and rotation of Asn233(190) occur upon inhibitor binding to the VIM-2 enzyme. In the crystal structure of the IMP-1−mercaptocarboxylate inhibitor complex,[22] a similar behavior was observed, where the carbonyl oxygen of the inhibitor is oriented for interaction with the side chain ND2 of Asn233(167) (4.1 Å) in an oxyanion hole.[31] From the above results it can be concluded that the role of Asn233(190) in the VIM-2 structure is to stabilize either a substrate or an inhibitor.

Conclusion

We determined the three-dimensional structure of a VIM-2 enzyme complexed with a mercaptocarboxylate inhibitor, phenylC3SH, which is the first VIM family member to be characterized as being complexed with an inhibitor. From the results of the crystal structure, the precise inhibition mode of the VIM-2 enzyme with phenylC3SH was ascertained: in particular, Phe61(42) and Tyr67(47), located in loop1 and Arg228(185) and Asn233(190) in loop2 play an important role in the binding and recognition of the inhibitor to the VIM-2 enzyme and in the stabilization of the VIM-2 structure. Moreover, Phe61 and Tyr67 residues are conserved in the other members of subclass B1 MBLs: VIM-1,[38] BlaB,[39] and IND-1.[40] Therefore, in these MBLs, two residues seem to play the same role, as can been seen in this study.

These findings would aid in the design of inhibitors that target not only VIM-2 but also other MBLs.

Experimental Section

Expression and Purification. The VIM-2 metallo-β-lactamse was expressed by *Escherichia coli* NCB326-1B2 harboring pVM4k/VIM-2 and purified as previously described.[30]

Synthesis of Inhibitor. *rac*-2-ω-Phenylpropyl-3-mercaptopropionic acid, phenylC3SH, was synthesized by the method described by Park et al.[41]

Crystallization of the VIM-2 Enzyme Complexed with PhenylC3SH. Prior to the X-ray diffraction experiments, a buffer solution of the VIM-2 enzyme was converted from Tris-HCl (50 mM, pH 7.4, 0.5 M NaCl) to HEPES−NaOH (20 mM, pH 7.5) and the VIM-2 protein was then concentrated to about 5 mg/mL (160 μM) on a Centricon. Drops of the VIM-2 protein with phenylC3SH were prepared by mixing 2 μL of a concentrated protein solution, 2 μL of a reservoir solution (30% PEG MME5000, 0.1 M MES−NaOH, and 0.2 M ammonium sulfate (pH 6.5)), and 1 μL of a methanolic phenylC3SH solution (10 mM). The crystals were grown for two months as plates (0.4 mm × 0.4 mm × 0.2 mm) at 20 C°.

Data Collection and Processing. Cocrystals of the VIM-2 enzyme with phenylC3SH were mounted in nylon loops directly from the mother liquor and flash-cooled in liquid nitrogen stream (100 K). All diffraction data were collected on beamline BL40B2 using an ADSC Quantum-4R detector at 100 K and beamline BL41XU using a marCCD 165 detector at 100 K at SPring-8 (Harima, Japan). A full MAD data collection around the zinc edge was performed with a single frozen crystal at SPring-8 BL40B2. Diffraction data were collected by the oscillation method at three carefully selected wavelengths: $\lambda_1 = 1.2826$ Å (edge, f''minimum), $\lambda_2 = 1.2817$ Å (peak, f'' maximum), and $\lambda_3 = 1.2906$ Å (remote high-energy wavelength). After completion of the MAD data collection at a resolution of 2.55 Å, a data set of 360 frames at $\lambda = 1.0000$ Å was collected at a resolution of 2.3 Å with 0.5° oscillation steps at SPring-8 BL41XU. The data were integrated and scaled with HKL2000.[42]

Phasing, Structure Determination, Model Building, and Refinement. Phase determination for the VIM-2 enzyme complexed with phenylC3SH was performed using the SOLVE program[43] and density modification, and model building was performed with the RESOLVE program.[44] This led to an interpretable density map and

an initial map. The O[45] and Coot[46] programs were further used in modeling and remodeling. The refinement was carried out using REFMAC5,[47] a component of the CCP4 suite,[48] and CNS[49] programs without a noncrystallographic symmetry (NCS). PhenylC3SH was built and minimized in MOE (CCG Inc., Canada), and the topology and parameter files of phenylC3SH were utilized in PRPDRG (http://davapc1.bioch.dundee.ac.uk/programs/prodrg/).[50] The quality of the model was inspected by the program PROCHECK.[51] Data collection and refinement statistics can be found in Table 1. The atomic coordinates and structure factors (PDB code 2YZ3) have been deposited at the Protein Data Bank, Research Collaboratory for Structural Bioinformatics, Rutgers University, New Brunswick, NJ (http://www.rcsb.org/).

In the case of the IMP-1 enzyme, however, we were unable to examine the IMP-1 enzyme complexed with phenylC3SH by X-ray crystallography because of the poor quality of the crystals obtained.

Acknowledgment. Work related to the preparation, purification, and X-ray crystallographical studies of the enzymes was supported by a Grant from the Ministry of Health, Labor, and Welfare of Japan (H18-Shinkou-11). The synthetic study was supported by a Grant-in-Aid for Scientific Research (B) (Grant No. 18390038) and Grant-in-Aid for Young Scientists (B) (Grant No. 18790028) from the Japan Society for the Promotion of Science.

References

(1) Cricco, J. A.; Vila, A. J. Class B β-lactamases: the importance of being metallic. *Curr. Pharm. Des.* **1999**, *5*, 915–927.
(2) Page, M. I. The reactivity of β-lactams, the mechanism of catalysis and the inhibition of β-lactamases. *Curr. Pharm. Des.* **1999**, *5*, 895–913.
(3) Ambler, R. P. The structure of β-lactamases. *Phil. Trans. R. Soc. London, Ser. B* **1980**, *289*, 321–331.
(4) Babic, M.; Hujer, A. M.; Bonomo, R. A. What's new in antibiotic resistance? Focus on beta-lactamases. *Drug Resist. Updates* **2006**, *9*, 142–156.
(5) Fisher, J. F.; Meroueh, S. O.; Mobashery, S. Bacterial resistance to β-lactam antibiotics: compelling opportunism, compelling opportunity. *Chem. Rev.* **2005**, *105*, 395–424.
(6) Galleni, M.; Lamotte-Brasseur, J.; Rossolini, G. M.; Spencer, J.; Dideberg, O.; Frère, J.-M. The metallo-β-lactamase working group Standard numbering scheme for class B β-lactamases. *Antimicrob. Agents Chemother.* **2001**, *45*, 660–663.
(7) Heinz, U.; Adolph, H.-W. Metallo-β-lactamases: two binding sites for one catalytic metal ion. *Cell. Mol. Life Sci.* **2004**, *61*, 2827–2839.
(8) Hussain, M.; Carlino, A.; Madonna, M. J.; Lampen, J. O. Cloning and sequencing of the metallothioprotein β-lactamase II gene of *Bacillus cereus* 569/H in *Escherichia coli*. *J. Bacteriol.* **1985**, *164*, 223–229.
(9) Walsh, T. R.; Toleman, M. A.; Poirel, L.; Nordmann, P. Metallo-β-lactamases: the quiet before the storm. *Clin. Microbiol. Rev.* **2005**, *18*, 306–325.
(10) Rasmussen, B. A.; Gluzman, Y.; Tally, F. P. Cloning and sequencing of the class B β-lactamase gene (*ccrA*) from *Bacteroides fragilis* TAL3636. *Antimicrob. Agents Chemother.* **1990**, *34*, 1590–1592.
(11) Massidda, O.; Rossolini, G. M.; Satta, G. The *Aeromonas hydrophila cphA* gene: molecular heterogeneity among class B metallo-β-lactamases. *J. Bacteriol.* **1991**, *173*, 4611–4617.
(12) Walsh, T. R.; Gamblin, S.; Emery, D. C.; MacGowan, A. P.; Bennett, P. M. Enzyme kinetics and biochemical analysis of ImiS, the metallo-β-lactamase from *Aeromonas sobria* 163a. *J. Antimicrob. Chemother.* **1996**, *37*, 423–431.
(13) Walsh, T. R.; Hall, L.; Assinder, S. J.; Nichols, W. W.; Cartwright, S. J.; MacGowan, A. P.; Bennett, P. M. Sequence analysis of the L1 metallo-β-lactamase from *Xanthomonas maltophilia*. *Biochim. Biophys. Acta* **1994**, *1218*, 199–201.
(14) Rossolini, G. M.; Condemi, M. A.; Pantanella, F.; Docquier, J.-D.; Amicosante, G.; Thaller, M. C. Metallo-β-lactamase producers in environmental microbiota: new molecular class B enzyme in *Janthinobacterium lividum*. *Antimicrob. Agents Chemother.* **2001**, *45*, 837–844.
(15) Poirel, L.; Naas, T.; Nicolas, D.; Collet, L.; Bellais, S.; Cavallo, J.-D.; Nordmann, P. Characterization of VIM-2, a carbapenem-hydrolyzing metallo-β-lactamase and its plasmid- and integron-borne gene from a *Pseudomonas aeruginosa* clinical isolate in France. *Antimicrob. Agents Chemother.* **2000**, *44*, 891–897.
(16) Moali, C.; Anne, C.; Lamotte-Brasseur, J.; Groslambert, S.; Devreese, B.; Van Beeumen, J.; Galleni, M.; Frère, J.-M. Analysis of the importance of the metallo-β-lactamase active site loop in substrate binding and catalysis. *Chem. Biol.* **2003**, *10*, 319–329.
(17) Huntley, J. J. A.; Scrofani, S. D. B.; Osborne, M. J.; Wright, P. E.; Dyson, H. J. Dynamics of the metallo-β-lactamase from *Bacteroides fragilis* in the presence and absence of a tight-binding inhibitor. *Biochemistry* **2000**, *39*, 13356–13364.
(18) Huntley, J. J.; Fast, W.; Benkovic, S. J.; Wright, P. E.; Dyson, H. J. Role of a solvent-exposed tryptophan in the recognition and binding of antibiotic substrates for a metallo-β-lactamase. *Protein Sci.* **2003**, *12*, 1368–1375.
(19) Scrofani, S. D. B.; Chung, J.; Huntley, J. J. A.; Benkovic, S. J.; Wright, P. E.; Dyson, H. J. NMR characterization of the metallo-β-lactamase from *Bacteroides fragilis* and its interaction with a tight-binding inhibitor: role of an active-site loop. *Biochemistry* **1999**, *38*, 14507–14514.
(20) Docquier, J.-D.; Lamotte-Brasseur, J.; Galleni, M.; Amicosante, G.; Frère, J.-M.; Rossolini, G. M. On functional and structural heterogeneity of VIM-type metallo-β-lactamases. *J. Antimicrob. Chemother.* **2003**, *51*, 257–266.
(21) Salsbury, F. R., Jr.; Crowley, M. F.; Brooks, C. L., III. Modeling of the metallo-β-lactamase from *B. fragilis*: structural and dynamic effects of inhibitor binding. *Proteins. Struct., Funct., Genet.* **2001**, *44*, 448–459.
(22) Concha, N. O.; Janson, C. A.; Rowling, P.; Pearson, S.; Cheever, C. A.; Clarke, B. P.; Lewis, C.; Galleni, M.; Frère, J.-M.; Payne, D. J.; Bateson, J. H.; Abdel-Meguid, S. S. Crystal structure of the IMP-1 metallo β-lactamase from *Pseudomonas aeruginosa* and its complex with a mercaptocarboxylate inhibitor: binding determinants of a potent, broad-spectrum inhibitor. *Biochemistry* **2000**, *39*, 4288–4298.
(23) Fitzgerald, P. M. D.; Wu, J. K.; Toney, J. H. Unanticipated inhibition of the metallo-β-lactamase from *Bacteroides fragilis* by 4-morpholineethanesulfonic acid (MES): a crystallographic study at 1.85-Å resolution. *Biochemistry* **1998**, *37*, 6791–6800.
(24) Toney, J. H.; Fitzgerald, P. M. D.; Grover-Sharma, N.; Olson, S. H.; May, W. J.; Sundelof, J. G.; Vanderwall, D. E.; Cleary, K. A.; Grant, S. K.; Wu, J. K.; Kozarich, J. W.; Pompliano, D. L.; Hammond, G. G. Antibiotic sensitization using biphenyl tetrazoles as potent inhibitors of *Bacteroides fragilis* metallo-β-lactamase. *Chem. Biol.* **1998**, *5*, 185–196.
(25) Toney, J. H.; Hammond, G. G.; Fitzgerald, P. M. D.; Sharma, N.; Balkovec, J. M.; Rouen, G. P.; Olson, S. H.; Hammond, M. L.; Greenlee, M. L.; Gao, Y.-D. Succinic acids as potent inhibitors of plasmid-borne IMP-1 metallo-β-lactamase. *J. Biol. Chem.* **2001**, *276*, 31913–31918.
(26) Kurosaki, H.; Yamaguchi, Y.; Higashi, T.; Soga, K.; Matsueda, S.; Yumoto, H.; Misumi, S.; Yamagata, Y.; Arakawa, Y.; Goto, M. Irreversible inhibition of metallo-β-lactamase (IMP-1) by 3-(3-mercaptopropionylsulfanyl)propionic acid pentafluorophenyl ester. *Angew. Chem., Int. Ed.* **2005**, *44*, 3861–3864.
(27) Kurosaki, H.; Yamaguchi, Y.; Yasuzawa, H.; Jin, W.; Yamagata, Y.; Arakawa, Y. Probing, inhibition, and crystallographic characterization of metallo-β-lactamase (IMP-1) with fluorescent agents containing dansyl and thiol groups. *ChemMedChem* **2006**, *1*, 969–972.
(28) García-Sáez, I.; Hopkins, J.; Papamicael, C.; Franceschini, N.; Amicosante, G.; Rossolini, G. M.; Galleni, M.; Frère, J.-M.; Dideberg, O. The 1.5-Å structure of *Chryseobacterium meningosepticum* zinc β-lactamase in complex with the inhibitor, D-captopril. *J. Biol. Chem.* **2003**, *278*, 23868–23873.
(29) García-Sáez, I.; Mercuri, P. S.; Papamicael, C.; Kahn, R.; Frère, J.-M.; Galleni, M.; Rossolini, G. M.; Dideberg, O. Three-dimensional structure of FEZ-1, a monomeric subclass B3 metallo-β-lactamase from *Fluoribacter gormanii*, in native form and in complex with D-captopril. *J. Mol. Biol.* **2003**, *325*, 651–660.
(30) Jin, W.; Arakawa, Y.; Yasuzawa, H.; Taki, T.; Hashiguchi, R.; Mitsutani, K.; Shoga, A.; Yamaguchi, Y.; Kurosaki, H.; Shibata, N.; Ohta, M.; Goto, M. Comparative study of the inhibition of metallo-β-lactamases (IMP-1 and VIM-2) by thiol compounds that contain a hydrophobic group. *Biol. Pharm. Bull.* **2004**, *27*, 851–856.
(31) Concha, N. O.; Rasmussen, B. A.; Bush, K.; Herzberg, O. Crystal structure of the wide-spectrum binuclear zinc β-lactamase from *Bacteroides fragilis*. *Structure* **1996**, *4*, 823–836.
(32) Carfi, A.; Pares, S.; Duée, E.; Galleni, M.; Duez, C.; Frère, J.-M.; Dideberg, O. The 3-D structure of a zinc metallo-β-lactamase from *Bacillus cereus* reveals a new type of protein fold. *EMBO J.* **1995**, *14*, 4914–4921.
(33) De La Sierra-Gallay, I. L.; Pellegrini, O.; Condon, C. Structural basis for substrate binding, cleavage and allostery in the tRNA maturase RNase Z. *Nature* **2005**, *433*, 657–661.
(34) Mandel, C. R.; Kaneko, S.; Zhang, H.; Gebauer, D.; Vethantham, V.; Manley, J. L.; Tong, L. Polyadenylation factor CPSF-73 is the pre-mRNA 3′-end-processing endonuclease. *Nature* **2006**, *444*, 953–956.

(35) Wang, Z.; Benkovic, S. J. Purification, characterization, and kinetic studies of a soluble *Bacteroides fragilis* metallo-β-lactamase that provides multiple antibiotic resistance. *J. Biol. Chem.* **1998**, *273*, 22402–22408.

(36) Wang, Z.; Fast, W.; Valentine, A. M.; Benkovic, S. J. Metallo-β-lactamase: structure and mechanism. *Curr. Opin. Chem. Biol.* **1999**, *3*, 614–622.

(37) Wang, Z.; Fast, W.; Benkovic, S. J. Direct observation of an enzyme-bound intermediate in the catalytic cycle of the metallo-β-lactamase from *Bacteroides fragilis*. *J. Am. Chem. Soc.* **1998**, *120*, 10778–10789.

(38) Lauretti, L.; Riccio, M. L.; Mazzariol, A.; Cornaglia, G.; Amicosante, G.; Fontana, R.; Rossolini, G. M. Cloning and characterization of bla_{VIM}, a new integron-borne metallo-β-lactamase gene from a *Pseudomonas aeruginosa* clinical isolate. *Antimicrob. Agents Chemother.* **1999**, *43*, 1584–1590.

(39) Rossolini, G. M.; Franceschini, N.; Riccio, M. L.; Mercuri, P. S.; Perilli, M.; Galleni, M.; Frère, J.-M.; Amicosante, G. Characterization and sequence of the *Chryseobacterium* (*Flavobacterium*) *meningosepticum* carbapenemase: a new molecular class B β-lactamase showing a broad substrate profile. *Biochem. J.* **1998**, *332*, 145–152.

(40) Bellais, S.; Léotard, S.; Poirel, L.; Naas, T.; Nordmann, P. Molecular characterization of a carbapenem-hydrolyzing β-lactamase from *Chryseobacterium* (*Flavobacterium*) indologenes. *FEMS Microbiol. Lett.* **1999**, *171*, 127–132.

(41) Park, J. D.; Kim, D. H. Cysteine derivatives as inhibitors for carboxypeptidase A: synthesis and structure−activity relationships. *J. Med. Chem.* **2002**, *45*, 911–918.

(42) Otwinowski, Z.; Minor, W. Processing of X-ray diffraction data collected in oscillation mode. *Methods Enzymol.* **1997**, *276*, 307–326.

(43) Terwilliger, T. C.; Berendzen, J. Automated MAD and MIR structure solution. *Acta Crystallogr., Sect. D: Biol. Crystallogr.* **1999**, *55*, 849–861.

(44) Terwilliger, T. C. Maximum-likelihood density modification. *Acta Crystallogr., Sect. D: Biol. Crystallogr.* **2000**, *56*, 965–972.

(45) Jones, T. A.; Zou, J.-Y.; Cowan, S. W.; Kjeldgaard, M. Improved methods for building protein models in electron density maps and the location of errors in these models. *Acta Crystallogr., Sect. A: Found. Crystallogr.* **1991**, *47*, 110–119.

(46) Emsley, P.; Cowtan, K. Coot: model-building tools for molecular graphics. *Acta Crystallogr., Sect. D: Biol. Crystallogr.* **2004**, *60*, 2126–2132.

(47) Murshudov, G. N.; Vagin, A. A.; Dodson, E. J. Refinement of macromolecular structures by the maximum-likelihood method. *Acta Crystallogr., Sect. D: Biol. Crystallogr.* **1997**, *53*, 240–255.

(48) Collaborative Computational Project Number 4. The CCP4 suite: programs for protein crystallography. *Acta Crystallogr., Sect. D: Biol. Crystallogr.* **1994**, *50*, 760–763.

(49) Brünger, A. T.; Adams, P. D.; Clore, G. M.; DeLano, W. L.; Gros, P.; Grosse-Kunstleve, R. W.; Jiang, J.-S.; Kuszewski, J.; Nilges, M.; Pannu, N. S.; Read, R. J.; Rice, L. M.; Simonson, T.; Warren, G. L. Crystallography & NMR system: a new software suite for macromolecular structure determination. *Acta Crystallogr., Sect. D: Biol. Crystallogr.* **1998**, *54*, 905–921.

(50) Schüttelkopf, A. W.; Van Aaltena, D. M. PRODRG: a tool for high-throughput crystallography of protein−ligand complexes. *Acta Crystallogr., Sect. D: Biol. Crystallogr.* **2004**, *6*, 1355–1363.

(51) Laskowski, R. A.; MacArthur, M. W.; Moss, D. S.; Thornton, J. M. PROCHECK: a program to check the stereochemical quality of protein structures. *J. Appl. Crystallogr.* **1993**, *26*, 283–291.

JM701031N